applied mechanics

MDPI

Article

Bending Stresses and Deformations in Prismatic Profiled Shafts with Noncircular Contours Based on Higher Hybrid Trochoids

Masoud Ziaei

Department of Mechanical Engineering and Automotive Engineering, Westsächsische Hochschule Zwickau, D-08056 Zwickau, Germany; masoud.ziaei@fh-zwickau.de

Abstract: This paper presents an analytical method for determining the bending stresses and deformations in prismatic, noncircular profile shafts with trochoidal cross sections. The so-called higher trochoids can be used as form-fit shaft-hub connections. Hybrid (mixed) higher trochoids (M-profiles) were developed for the special application as a profile contour for the form-fit shaft and hub connections in an earlier work by the author. M-profiles combine the advantages of the two standardised polygonal and spline contours, which are used as shaft-hub connections for the transmission of high torques. In this study, the geometric and mechanical properties of the higher hybrid trochoids were investigated using complex functions to simplify the calculations. The pure bending stress and shaft deflection were determined for M-profiles using bending theory based on the theory of mathematical elasticity. The loading cases consisted of static and rotating bends. Analytical, numerical, and experimental results agreed well. The calculation formulas developed in this work enable reliable and low-cost dimensioning with regard to the stresses and elastic deformations of profile shafts subjected to bending loads.

Keywords: higher trochoids; noncircular cross sections; profiled shafts; form-fit shaft and hub connections; bending stress; bending deflection; rotating bending stress

Citation: Ziaei, M. Bending Stresses and Deformations in Prismatic Profiled Shafts with Noncircular Contours Based on Higher Hybrid Trochoids. *Appl. Mech.* **2022**, *3*, 1063–1079. https://doi.org/10.3390/applmech3030060

Received: 28 June 2022
Accepted: 17 August 2022
Published: 23 August 2022

1. Introduction

In recent years, the noncircular profiles have been increasingly incorporated in industrial applications as form-fitting shaft-hub connections. These profiles have a higher transmission capacity than the commercially available connections such as press and key connections.

The so-called higher trochoids can be used as form-fit shaft–hub connections. Hybrid (mixed) higher trochoids (M-profiles) were proposed in [1] and adapted to a practical industrial application in [2]. M-profiles combine the advantages of standardised polygon (DIN 32711 [3]) and spline (DIN 5486 [4]) contours used as shaft–hub connections for the transmission of torsional loads.

A new German standard for hypotrochoidal profiled connections (H-profiles) was published in 2021 (DIN 3689 T-1 [5]). Furthermore, new noncircular profiles were developed, investigated, and optimized on the ground of the higher trochoids in research projects at the West Saxony University of Zwickau, Germany [1,2]. Higher trochoids are classified into three main profile families. Hybrid trochoids (M-profiles) are well adaptable to an arbitrary construction space.

In many practical applications, the shaft fails outside of the connection due to bending stresses. For such cases, the analytical approaches may be cheaper and more reliable than numerical methods. The geometrical and mechanical properties of the higher trochoids can be formulated using the complex functions.

According to Muskhelishvili [6], conformal mapping enables the derivation of analytical solutions for bending stresses. For the solution of pure bending, only a conformal mapping of the profile contour is adequate. However, a complete mapping of the profile cross-section is necessary for the shear force bending.

2. Geometry of Higher Trochoids

Higher trochoids were treated systematically for the first time by Wunderlich [7] and are represented by complex functions. Thus, the two-parameter equations can be combined into one complex equation, reducing the mathematical effort. This approach was used in [8] for a plane–curve representation. As shown in Figure 1, K_S is defined by the planetary motion of several levers with corresponding angular velocities $\omega_1, \omega_2, \cdots \omega_s$. The position of the point A_S is determined by the sum of the vectors $\vec{A_0A_1}, \vec{A_1A_2}, \cdots \vec{A_{S-1}A_S}$ and can be expressed as follows:

$$\omega(\mathrm{e}^{i\,t}) = r \cdot \mathrm{e}^{i\,\omega_0\,t} + e_1 \cdot \mathrm{e}^{i\,\omega_1\,t} + e_2 \cdot \mathrm{e}^{i\,\omega_2\,t} + \cdots = r \cdot \mathrm{e}^{i\,\omega_0\,t} + \sum_{j=1}^{S} e_j \cdot \mathrm{e}^{i\,\omega_j\,t} \tag{1}$$

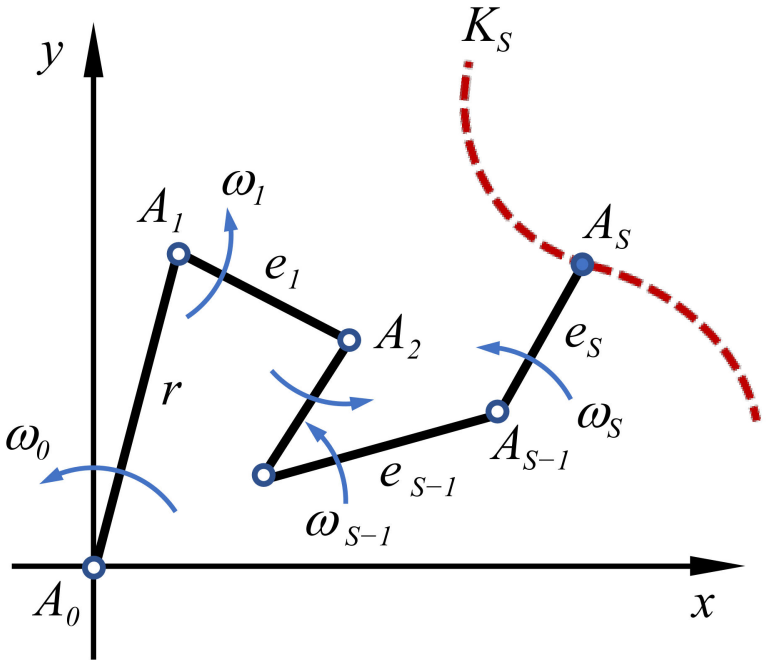

Figure 1. Definition of the higher trochoid [7].

Here, e represents Euler's number and $i = \sqrt{-1}$ denotes an imaginary unit. The first radius r is defined as the main radius and the levers $e_1, e_2, \cdots e_s$ are used to describe the eccentricities of the profile. Point A_S is assumed to be the generating point. For simplicity, e^{it} has been replaced with ζ, yielding the following general form for higher trochoids:

$$\omega(\zeta) = r \cdot \zeta^{\omega_0} + e_1 \cdot \zeta^{\omega_1} + e_2 \cdot \zeta^{\omega_2} + \cdots = r \cdot \zeta^{\omega_0} + \sum_{j=1}^{s} e_j \cdot \zeta^{\omega_j}. \tag{2}$$

If any e-lever shown in Figure 1 rotates on its own plane, an arbitrary point on the corresponding plane can be selected as the pivot point for the next plane. The 'extended' or 'shortened' higher trochoidal curves can be generated using Equation (2), depending on the distance between a selected point and its pivot point. Closed curves with periodic symmetry are typically useful for technical applications. However, the ratios of the angular velocities ω_j are not freely selectable for such curves.

Higher trochoidal curves are classified into the following three families ([9]):

- **Higher epitrochoids**

  Consider the following conditions:

  - angular velocities ω_j act in the same (positive) direction and

- $r > 0, \omega_1 = 1 + n, \omega_2 = 1 + 2n, \cdots \omega_s = 1 + 2s \cdot n$, where $n \geq 1$ is an arbitrary integer.

Equation (2) leads to the following relationship:

$$\omega(\zeta) = r \cdot \zeta + e_1 \cdot \zeta^{n+1} + e_2 \cdot \zeta^{2n+1} + \cdots + e_s \cdot \zeta^{s \cdot n+1} = r \cdot \zeta + \sum_{j=1}^{s} e_j \cdot \zeta^{jn+1}. \quad (3)$$

Equation (3) describes the higher epitrochoids of the nth order.

- **Higher hypotrochoids**

Consider the following conditions:

- angular velocities ω_j act in the same (negative) direction and
- $r > 0, \omega_{-1} = 1 - n, \omega_{-2} = 1 - 2n, \cdots \omega_{-s} = 1 - 2s \cdot n$, where $n \geq 3$ is an arbitrary integer.

Equation (2) leads to the following relationship:

$$\omega(\zeta) = r \cdot \zeta + e_{-1} \cdot \zeta^{1-n} + e_{-2} \cdot \zeta^{1-2n} + \cdots + e_{-s} \cdot \zeta^{1-s \cdot n} = r \cdot \zeta + \sum_{j=1}^{s} e_{-j} \cdot \zeta^{1-jn}. \quad (4)$$

Equation (4) describes the higher hypotrochoids of the nth order.

- **Higher hybrid (mixed) trochoid**

Considering the following conditions:

- angular velocities ω_j act in positive or negative directions and
- $r > 0, \omega_{-1} = 1 - n, \omega_{-2} = 1 - 2n, \cdots \omega_{-s} = 1 - 2s \cdot n$ as well as $\omega_1 = 1 + n$, $\omega_2 = 1 + 2n, \cdots \omega_s = 1 + 2s \cdot n$, where $n \geq 3$ is an arbitrary integer.

Equation (2) leads to the following relationship, which describes higher hybrid (mixed) trochoids:

$$\begin{aligned} \omega(\zeta) \quad &= e_{-s} \cdot \zeta^{1-s \cdot n} + \cdots + e_{-2} \cdot \zeta^{1-2n} + e_{-1} \cdot \zeta^{1-n} + r \cdot \zeta + e_1 \cdot \zeta^{n+1} + e_2 \cdot \\ &\zeta^{2n+1} + \cdots + e_s \cdot \zeta^{s \cdot n+1} = r \cdot \zeta + \sum_{j=1}^{s} \left(e_{-j} \cdot \zeta^{1-jn} + e_j \cdot \zeta^{jn+1} \right). \end{aligned} \quad (5)$$

This trochoid has an order of $2 \cdot s - 1$. In essence, Equation (5) is the sum of Equations (3) and (4), where the term $r \cdot \zeta$ is considered only once.

For all three classes of curves, n describes the periodicity of the trochoid; therefore, it also represents the number of sides of the profile whose boundary contour is described by the corresponding equation.

Hybrid trochoidal profiles were also presented in [9], where two real parameter functions were used to describe the geometry. Using the above methodology, the contour geometry can be determined via a single 'complex' equation, simplifying the investigations of a profile's geometric and mechanical properties. If the function $\omega(\zeta)$ conformably maps the boundary of a unit circle to the profile contour, the complex formulation should facilitate the investigation of the mechanical stresses in the profiles [6,10]. In [11,12], such formulations were used to solve the torsion problem for prismatic profile shafts.

Special features of higher hybrid (M) profiles

This study deals with the general description of hybrid (M) profiles based on Equation (5). By changing the periodicity n and the number of e values and their sign, innumerable profile contours can be obtained that can be adapted to any technical application.

Figure 2 presents examples of M-profiles, where m represents the order of the profile. A change in the e values may produce concave, flat, or convex flanks while the general profile character remains unchanged.

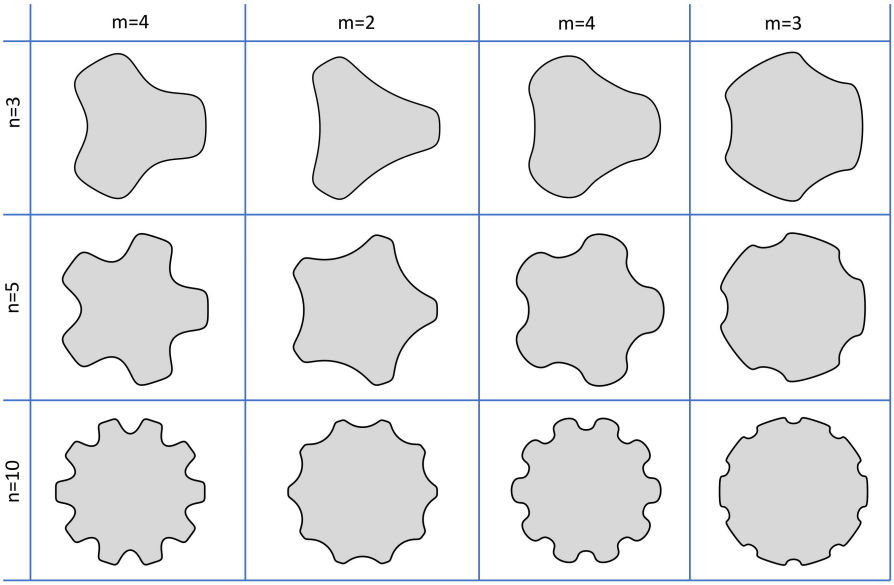

Figure 2. Examples of the complex hybrid trochoid (M-profiles) with additional eccentricities, where m represents the order and n represents the periodicity of the profile.

3. Geometric Properties of M-Profiles

According to the contour $\omega(\zeta)$ based on Equation (5), the geometric properties of the profile, that is, the profile area, radii of the head circle (r_a) and foot circle (r_f), the contour curvatures, ρ, and the tooth height h can be determined. These variables determine the influences on the construction-space requirements and the profile form/friction-fit properties for application as a shaft–hub connection.

Figure 3 shows an example of the geometry sizes for an M-profile with eight teeth. The profile geometry can be changed depending on the eccentricities and adapted to predefined geometric conditions.

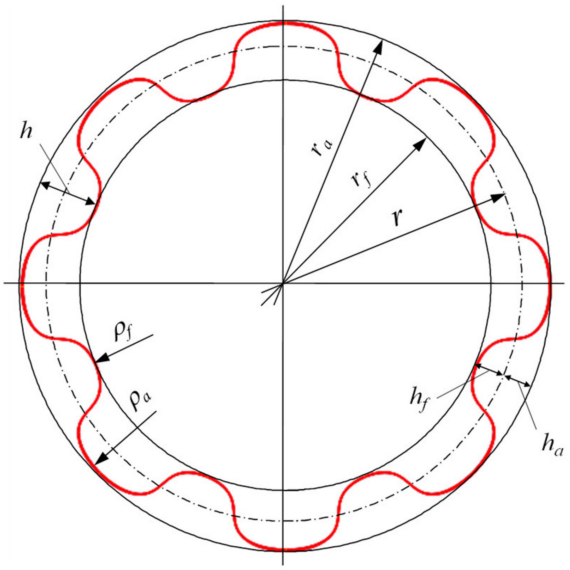

Figure 3. Geometry of the M-T04 family for n = 8 (exemplary) [1].

3.1. Area

The area enclosed by the contour $\omega(\zeta)$ can be determined as follows [8]:

$$\begin{array}{c} A = \frac{1}{2}\int_0^{2\pi} Im\left[\overline{\omega}(\zeta)\cdot\dot{\omega}(\zeta)\right]dt \text{ or :} \\ A = \frac{1}{2}\int_0^{2\pi} Im\left[i\cdot\omega\left(e^{-it}\right)\cdot\frac{d\omega\left(e^{it}\right)}{de^{it}}\cdot e^{it}\right]dt, \end{array} \tag{6}$$

where *Im*[ ] indicates the imaginary part of the function, which is presented in square brackets.

3.2. Radii of Head Circle (r_a) and Foot Circle (r_f)

By substituting $\zeta = e^{it}$ into Equation (5), the following relationship is obtained:

$$\begin{array}{l} \omega\left(e^{it}\right) = e_{-s}\cdot e^{(1-s\cdot n)it} + \cdots + e_{-2}\cdot e^{(1-2n)it} + e_{-1}\cdot e^{(1-n)it} + r\cdot e^{it} + e_1\cdot e^{(1+n)it} + \\ e_2 e^{(1+2n)it} + \cdots + e_s\cdot e^{(1+s\cdot n)it} = r\cdot e^{it} + \sum\limits_{j=1}^{s}\left(e_{-j}\cdot e^{(1-j\cdot n)it} + e_j\cdot e^{(1+j\cdot n)it}\right) \end{array} \tag{7}$$

Equation (7) describes the profile contour as a 'complex' function of the parameter angle t. If t = 0 is inserted into Equation (6), the radius of the head circle r_a is determined as follows:

$$\begin{array}{l} r_a = \left|\omega\left(e^{it}\right)\right|_{t=0} \\ = \left|e_{-s}\cdot e^{i(1-s\cdot n)t} + \cdots + e_{-1}\cdot e^{i(1-n)t} + r\cdot e^{it} + e_1\cdot e^{i(1+n)t} + \cdots + e_s e^{i(1+s\cdot n)t}\right|_{t=0}, \end{array}$$

that is,

$$r_a = r + \sum\nolimits_{j=1}^{s}\left(e_j + e_{-j}\right). \tag{8}$$

The radius of the foot circle r_f can be determined by substituting $t = \frac{\pi}{n}$ into Equation (7):

$$\begin{array}{l} r_f = \omega\left(e^{it}\right)\big|_{t=\frac{\pi}{n}} = e_{-s}\cdot e^{i\frac{(1-s\cdot n)\pi}{n}} + \cdots + e_{-1}\cdot e^{i\frac{(1-n)\pi}{n}} + r\cdot e^{i\frac{\pi}{n}} + e_1\cdot e^{i\frac{(1+n)\pi}{n}} + \cdots + e_s \\ e^{i\frac{(1+s\cdot n)\pi}{n}}, \end{array}$$

that is,

$$r_f = r + \sum_{j=1}^{s}(-1)^j\left(e_{-j} + e_j\right). \tag{9}$$

3.3. Tooth Height

Similar to the terminology of gear technology, the tooth height h can be defined for M-profiles. It is defined as the sum of the addendum h_a and dedendum h_f, as follows (see also Figure 3):

$$h = h_a + h_f = r_a - r_f, \tag{10}$$

where $h_a = r_a - r$ and $h_f = r - r_f$ are applied.

3.4. Radius of Curvature

The radius of curvature can then be determined from the elementary differential geometry in complex form as follows [8]:

$$\rho = 2i\cdot\frac{\left(\dot{\omega}\cdot\overline{\dot{\omega}}\right)^{\frac{3}{2}}}{\overline{\dot{\omega}}\cdot\ddot{\omega} - \dot{\omega}\cdot\overline{\ddot{\omega}}} = \frac{\left|\dot{\omega}\right|^3}{Im(\overline{\dot{\omega}}\cdot\ddot{\omega})}. \tag{11}$$

The following relations hold for the functions $\overline{\dot{\omega}}$ and $\overline{\ddot{\omega}}$:

$$\begin{aligned}\overline{\dot{\omega}} &= -\tfrac{i}{\zeta}\omega'(\zeta)\tfrac{i}{\zeta}'(\tfrac{1}{\zeta})\\ \overline{\ddot{\omega}} &= -\tfrac{1}{\zeta}\left(\omega''\left(\tfrac{1}{\zeta}\right)\tfrac{1}{\zeta}+\omega'\left(\tfrac{1}{\zeta}\right)\right)\ (\text{with } \zeta = e^{it}).\end{aligned} \tag{12}$$

The radii of curvature at the contour head and foot areas (ρ_a and ρ_f, respectively) are important for profile manufacturing and can be determined from Equation (10) with $t = 0$ and $t = \pi/n$, respectively.

4. M-Profiles with Four Eccentricities [1,2]

This effort aimed to combine the advantages of P3G profiles of DIN 32711 [3] (low form/notch coefficient) with those of the splined shaft profiles of DIN 5486 [4] (high form fit) in one profile. The M-profile contours were extensively investigated and optimised in [1] with regard to torsional loading. To keep the scope of the investigations manageable, profile families are developed with four eccentricities while maintaining the adaptability of the contour to practical applications.

The following contour description applies to an M-profile with s = 2 (or 4 eccentricities):

$$\begin{aligned}\omega\left(e^{it}\right) &= r\cdot e^{it}+\textstyle\sum_{j=1}^{2}\left(e_{-j}\cdot e^{(1-j\cdot n)it}+e_j\cdot e^{(1+j\cdot n)it}\right), \text{thatis,}\\ \omega(\zeta) &= e_{-2}\cdot\zeta^{1-2n}+e_{-1}\cdot\zeta^{1-n}+r\cdot\zeta+e_1\cdot\zeta^{1+n}+e_2\cdot\zeta^{1+2n}.\end{aligned} \tag{13}$$

Area

Accordingly, Equation (6) gives the following relationship for the area of the profile cross-section:

$$A = \pi\left[r^2-(2n-1)e_{-2}^2-n\left(e_{-1}^2-e_1^2-2e_2^2\right)+e_{-1}^2+e_1^2+e_2^2\right]. \tag{14}$$

Head circle

In many practical applications, the head circle determines the installation space of the profile. The radius of the head circle can be determined from the contour equation (Equation (13)) for the contour head (at $t = 0$) as follows:

$$\begin{aligned}r_a &= \left|\omega\left(e^{it}\right)\right|_{t=0} = \left|e_{-2}\cdot e^{i(1-2n)t}+e_{-1}\cdot e^{i(1-n)t}+r\cdot e^{it}+e_1\cdot e^{i(1+n)t}+e_2\cdot e^{i(1+2n)t}\right|_{t=0}\\ r_a &= r+e_1+e_2+e_{-1}+e_{-2}.\end{aligned} \tag{15}$$

Foot circle

As another characteristic, the foot-circle radius can be determined from Equation (13) with $t = \pi/2$, as follows:

$$\begin{aligned}r_f &= \left|\omega\left(e^{it}\right)\right|_{t=\frac{\pi}{n}} = \left|e_{-2}\cdot e^{i\frac{(1-2n)\pi}{n}}+e_{-1}\cdot e^{i\frac{(1-n)\pi}{n}}+r\cdot e^{i\frac{\pi}{n}}+e_1\cdot e^{i\frac{(1+n)\pi}{n}}+e_2\cdot e^{i\frac{(1+2n)\pi}{n}}\right|\\ r_f &= r-e_1+e_2-e_{-1}+e_{-2}.\end{aligned} \tag{16}$$

Tooth height

The tooth height is calculated as the difference between the radius of the head circle and that of the foot circle:

$$h = r_a - r_f = 2(e_1+e_{-1}). \tag{17}$$

The addendum and the dedendum are determined as follows:

$$h_a = r_a - r = e_1+e_2+e_{-1}+e_{-2} \tag{18}$$

$$h_f = r - r_f = e_1-e_2+e_{-1}-e_{-2}. \tag{19}$$

As indicated by Equation (17), the tooth height h depends only on e_1 and e_{-1}. According to Equations (18) and (19), the corresponding proportions h_a and h_f also depend on e_2 and e_{-2}.

Radius of curvature

The radii of curvature for the head and foot areas are determined using Equation (11) as follows:

$$\rho_a = -\frac{(r + e_2 - e_{-1} + e_{-2} + 2e_2 n + e_{-1} n - 2e_{-2} n - e_1(n+1))^2}{r - e_{-1} + e_{-2} + 2e_{-1} n - 4e_{-2} n - e_{-1} n^2 + 4e_{-2} n^2 - e_1(n+1)^2 + e_2(2n+1)^2} \quad (20)$$

$$\rho_f = \frac{(r + e_1 + e_2 + e_{-1} + e_{-2} + e_1 n + 2e_2 n - e_{-1} n - 2e_{-2} n)^2}{r + e_{-1} + e_{-2} - 2e_{-1} n - 4e_{-2} n + e_{-1} n^2 + 4e_{-2} n^2 + e_1(1+n)^2 + e_2(2n+1)^2}. \quad (21)$$

ρ_a plays an important role in selecting a suitable manufacturing method and can be adjusted by considering the eccentricity values in Equation (12). The concavity of the profile flank (and consequently the form-fit degree of the profile) can be determined using ρ_f in Equation (21).

M-T04 Profiles

In [1], the four simplified eccentricities e_{-2}, e_{-1}, e_1, and e_2 were defined as functions of a basic or main eccentricity e_0 to narrow the range of variants. The general form of Equation (13) was used as a basis, and extensive investigations were performed on the load-bearing capacities of profiles with a hub for torsional loading [1,13,14]. The eccentricities e_{-2}, e_{-1}, e_1, and e_2 are expressed as follows:

$$e_{-2} = -\frac{2n+1}{8} e_0,\ e_{-1} = \frac{n+1}{2} e_0,\ e_1 = (n-1) e_0,\ e_2 = \frac{2n-1}{8} e_0. \quad (22)$$

This results in the following contour description for the M-T04 profile family:

$$\omega(\zeta) = -\frac{2n+1}{8} e_0 \cdot \zeta^{1-2n} + \frac{n+1}{2} e_0 \cdot \zeta^{1-n} + r \cdot \zeta + (n-1) e_0 \cdot \zeta^{1+n} + \frac{2n-1}{8} e_0 \cdot \zeta^{1+2n} \quad (23)$$

The corresponding parametric equations can be obtained as follows:

$$\begin{aligned} x &= \left(r + e\left(\tfrac{3n-1}{2}\cos(nt) - \tfrac{n}{4}\cos(2nt)\right)\right)\cos(t) - e\left(\tfrac{n-3}{2}\sin(nt) + \tfrac{n}{2}\sin(2nt)\right)\sin(t) \\ y &= \left(r + e\left(\tfrac{3n-1}{2}\cos(nt) - \tfrac{n}{4}\cos(2nt)\right)\right)\sin(t) + e\left(\tfrac{n-3}{2}\sin(nt) + \tfrac{n}{2}\sin(2nt)\right)\cos(t) \end{aligned} \quad (24)$$

An analytical approach for resolving the torsion issue using conformal mappings was comprehensively presented in [1]. Figure 4 shows the testbench for the torsional load (left) and the cracking due to torsional loading (right) for the M-04-Profile studied in [1].

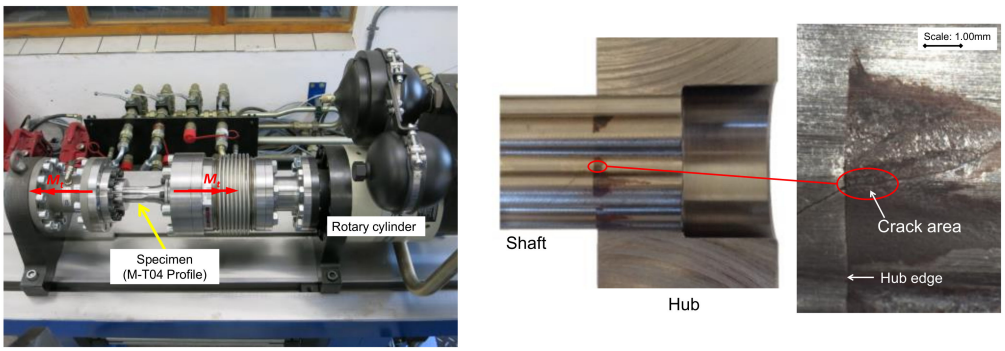

Figure 4. Testbench for the torsional load (**left**) and the cracking due to torsional loading (**right**) [1].

Geometric properties of M-T04 profiles

From Equation (14), the area enclosed by the M-T04 contour can be easily derived for any number of sides n, and the corresponding main eccentricity e_0:

$$A = \pi r^2 + \frac{\pi}{32} e_0^2 \left(24n^3 - 44n^2 - 24n + 41\right). \quad (25)$$

Additionally, Equations (15) and (16) can be used to calculate the radii of the head and foot circles as follows:

$$r_a = r + \sum_{j=1}^{s}\left(e_j + e_{-j}\right) = r + \frac{3}{4}e_0\ (2n-1) \tag{26}$$

$$r_f = r + \sum_{j=1}^{s}(-1)^j\left(e_{-j} + e_j\right) = r - \frac{1}{4}e_0(6n-1). \tag{27}$$

The tooth height h and its distribution can be determined from the parameter equations as functions of n and

$$h = e_0(3n-1),\ h_a = \frac{3e_0}{4}(2n-1),\ h_f = \frac{e_0}{4}(6n-1). \tag{28}$$

Additionally, the radii of the contour head and foot can be determined as follows:

$$\rho_a = \frac{\left(4r + 6e_0n^2 - 3e_0\right)^2}{16r + 4e_0(6n^3 + 6n^2 - 6n - 3)} \tag{29}$$

$$\rho_f = \frac{\left(4r + 2en^2 + e_0\right)^2}{16r - 4e_0(6n^3 - 2n^2 - 6n - 1)}. \tag{30}$$

5. Bending Stresses in Profiled Shaft

5.1. General Theory: Pure Bending

For prismatic beams with an arbitrary cross-section, the elementary approach can be used to solve for pure bending. Figure 5a schematically represents a prismatic beam subjected to a bending load with a noncircular cross-section and five teeth.

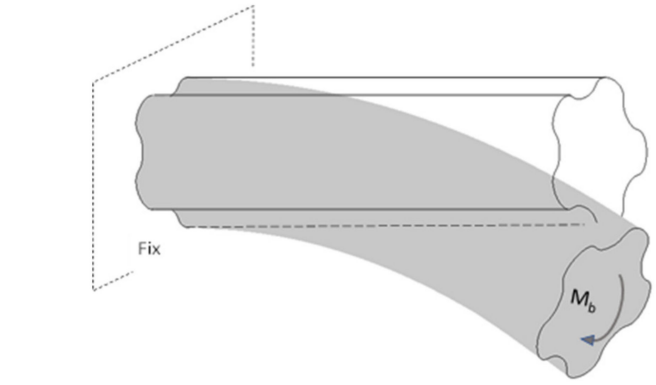

(**a**)

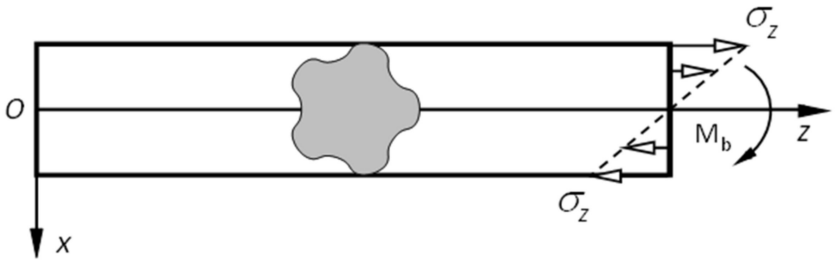

(**b**)

Figure 5. (**a**) Prismatic beam with a noncircular cross-section under pure bending; (**b**) coordinate system used to describe bending stresses.

Bending stress

Figure 5b presents the coordinate system used to describe the stresses in this study. The z-axis was set along the length of the shaft, and the x-axis was set in the vertical direction. The shaft was fixed to the left. For convenience, the coordinate origin was placed at the centre of gravity of the left profile face. To solve this problem, the following elementary approach from the literature is used, where the equilibrium and compatibility conditions for the elastic bodies are satisfied [6]:

$$\sigma_z = a \cdot x, \sigma_x = \sigma_y = \tau_{xy} = \tau_{zx} = \tau_{zy} = 0. \tag{31}$$

It is assumed that the plane cross sections remain planar upon loading. The factor a in Equation (31) represents a constant value determined by the equilibrium of the bending stresses. The resulting moment of the stresses acting on the right side (or on any cross-section) remains in equilibrium with the bending load with respect to the y-axis:

$$M_b = -\iint_S \sigma_z \cdot x dx dy. \tag{32}$$

Substituting σ_z from Equation (31) into (32) yields the following relationship, where I_y represents the moment of inertia of the profile section with respect to the y-axis:

$$M_b = -a \iint_S x^2 dx dy = -a \cdot I_y. \tag{33}$$

Therefore, the following relationship is valid:

$$a = -\frac{M_b}{I_y} \text{ or } \sigma_z = -\frac{M_b}{I_y} \cdot x. \tag{34}$$

Thus, the solution for the stresses can be obtained as follows:

$$\sigma_x = \sigma_y = \tau_{xy} = \tau_{yz} = \tau_{xz} = 0, \ \sigma_z = -\frac{M_b}{I_y} \cdot x. \tag{35}$$

Deflection

Displacements are determined using Hooke's law and the corresponding relation between displacements and strain as follows [6,10]:

$$\begin{array}{l} u_x = \frac{M_b}{2 \cdot E \cdot I_y} \cdot \left[z^2 + \nu \cdot \left(y^2 - x^2\right)\right] \\ u_y = -\frac{M_b \cdot \nu}{E \cdot I_y} \cdot (xy) \\ u_z = -\frac{M_b}{E \cdot I_y} \cdot (xz). \end{array} \tag{36a}$$

The deflection of the neutral axis is determined from u_x for $x = y = 0$, as follows:

$$\delta_x = \frac{M_b}{2 \cdot E \cdot I_y} \cdot z^2 \tag{36b}$$

$$\delta_x(z) = \frac{M_b}{2 \cdot E \cdot I_y} \cdot z^2. \tag{36c}$$

Bending moment of inertia

Although the moments of inertia usually involve a double integral over the profile cross-section, this is reduced to a simple curvilinear integral over the profile contour using Green's theorem, as follows [10]:

$$\begin{array}{l} I_x = -\frac{1}{3} \int_\gamma y^3 dx \\ I_y = \frac{1}{3} \int_\gamma x^3 dy \\ I_{xy} = \frac{1}{2} \int_\gamma x^2 y dy. \end{array} \tag{37}$$

The corresponding contour description based on Equation (13) is also advantageous. Cartesian coordinates can be easily obtained via elementary calculations using the complex functions, as follows (see [15]):

$$\begin{aligned} x &= \frac{\omega(\lambda)+\overline{\omega(\lambda)}}{2}, \\ y &= \frac{\omega(\lambda)-\overline{\omega(\lambda)}}{2\cdot i} \end{aligned} \tag{38}$$

By substituting Equation (38) into the definitions of the moments of inertia (Equation (37)), they are determined as follows, where $\lambda = e^{it}$ holds.

$$\begin{aligned} I_x &= -\tfrac{i}{48}\int_\gamma \left(\omega(\lambda)-\overline{\omega(\lambda)}\right)^3 d\left(\omega(\lambda)+\overline{\omega(\lambda)}\right) \\ I_y &= \tfrac{i}{48}\int_\gamma \left(\omega(\lambda)+\overline{\omega(\lambda)}\right)^3 d\left(\omega(\lambda)-\overline{\omega(\lambda)}\right) \\ I_{xy} &= -\tfrac{1}{32}\int_\gamma \left(\omega(\lambda)+\overline{\omega(\lambda)}\right)^2 \left(\omega(\lambda)-\overline{\omega(\lambda)}\right) d\left(\omega(\lambda)-\overline{\omega(\lambda)}\right) \end{aligned} \tag{39}$$

Equation (39) facilitates the determination of the moments of inertia when $\omega(\zeta)$ is available for the profile contour.

Rotational bending

Because a prismatic bar has technical applications as a rotating profile shaft, the bending moment of inertia should also be determined for rotated coordinates. Figure 6 schematically represents an M-04 profile with six teeth in Cartesian coordinates.

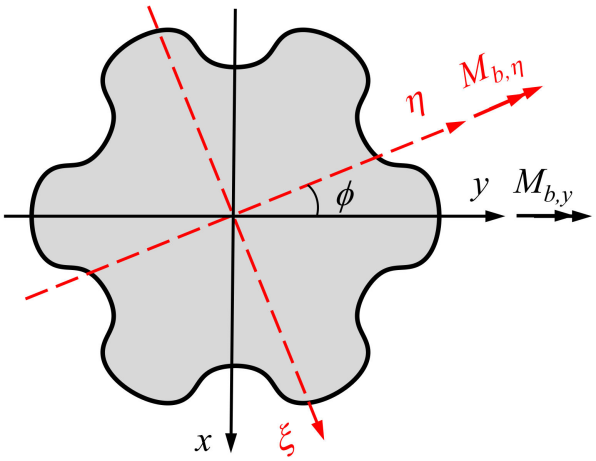

Figure 6. Rotated coordinate system for the profile cross-section.

The coordinates rotated by angles ϕ are denoted as ξ and η. Owing to the tensorial property of moments of inertia, the following relationships are obtained for the rotated coordinate system using Mohr's circle (see [16]):

$$\begin{aligned} I_\xi &= \tfrac{I_x+I_y}{2} + \tfrac{I_x-I_y}{2}\cos(2\phi) - I_{xy}\sin(2\phi) \\ I_\eta &= \tfrac{I_x+I_y}{2} - \tfrac{I_x-I_y}{2}\cos(2\phi) + I_{xy}\sin(2\phi) \\ I_{\xi\eta} &= \tfrac{I_x-I_y}{2}\sin(2\phi) + I_{xy}\cos(2\phi). \end{aligned} \tag{40}$$

The moments of inertia remain invariant owing to the periodic symmetry of the cross-section of the M-contours presented in this paper based on Equation (13). Therefore, the following relationships are valid from Equation (39):

$$I_x = I_y \text{ and } I_{xy} = 0. \tag{41}$$

This property is advantageous when Equation (39) is used to determine the moments of inertia for the rotated cross-section. By substituting the values from Equation (38) into Equation (37) for an arbitrary rotation angle ϕ, the following relationships are obtained:

$$\begin{array}{c} I_\xi = I_\eta (= I_x = I_y) \\ I_{\xi\eta} = I_{xy} = 0. \end{array} \tag{42}$$

The polar moment of inertia can be determined as follows:

$$I_p = 2 \cdot I_x = 2 \cdot I_y. \tag{43}$$

5.2. General Solution for M-T04 Profiles

Moments of inertia

By substituting the eccentricities from Equation (23) into Equation (39), the following equations are obtained for the moments of inertia for any number of flanks n and an arbitrary main eccentricity e_0:

$$\begin{array}{c} I_x = I_y = \frac{\pi}{4}\Big[r^4 + \frac{1}{16}e_0^2(24n^3 + 28n^2 - 72n + 51)r^2 + \frac{3}{8}e_0^3(6n^4 - 3n^3 - 7n^2 + 3n1)r \\ + \frac{3}{2048}e_0^4(768n^5 - 2096n^4 + 1440n^3 + 296n^2 - 2016n + 1473)\Big], \\ I_{xy} = 0. \end{array} \tag{44}$$

Then, according to Equation (43), the following relationship for the polar moment of inertia is valid:

$$\begin{array}{c} I_p = \frac{\pi}{2}\Big[r^4 + \frac{1}{16}e_0^2(24n^3 + 28n^2 - 72n + 51)r^2 + \frac{3}{8}e_0^3(6n^4 - 3n^3 - 7n^2 + 3n + 1)r + \\ \frac{3}{2048}e_0^4(768n^5 - 2096n^4 + 1440n^3 + 296n^2 - 2016n + 1473)\Big]. \end{array} \tag{45}$$

Therefore, the bending stress and deformations can be determined using Equations (35) and (36), respectively.

Bending stress

To obtain a general solution for the bending stress σ_z based on (35), lever x should be converted to the rotated coordinate system:

$$\xi = y\cos(\phi) - x\sin(\phi), \tag{46}$$

where ϕ represents the rotation angle. If the values of x and y from Equation (24) are substituted into Equation (46), the following relationship is obtained for the rotated coordinate ξ on the profile contour ($0 \le t \le 2\pi$):

$$\xi(\phi, t) = \frac{2e_0(n - 3 + 2n\cos(nt))\cos(t - \phi)\sin(nt) + (4r + 2e_0(3n - 1)\cos(nt) - e_0\cos(2nt))\sin(t - \phi)}{4}. \tag{47}$$

The distribution of bending stress on the profile contour can be determined using the following equation:

$$\sigma_z(\phi, t) = -\frac{M_b}{I_\eta} \cdot \xi(\phi, t). \tag{48}$$

By substituting ξ from Equation (47) and I_y from Equation (44) into Equation (48), the distribution of the bending stress on the profile contour can be determined.

5.3. M-04 Profile from [1]

As an example, the profile experimentally investigated in [1] for torsional loading (see Figure 4) was used as a basis to investigate the bending behaviour. The corresponding

geometric properties are $n = 6, r = 17.44$ mm, and $e_0 = 0.3104$ mm (Figure 7). Equation (23) provides the following relationship for the contour of this profile:

$$\omega(\zeta) = -\frac{0.504}{\zeta^{11}} + \frac{1.086}{\zeta^5} + 17.44\zeta + 1.552\zeta^7 + 0.427\zeta^{13}. \tag{49}$$

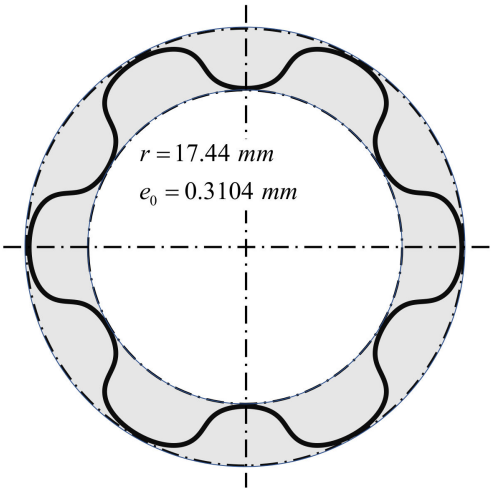

Figure 7. Investigated M-T04 profiles in [1].

The bending moment of inertia about the x- or y-axis of $I_x = I_y = 82113$ mm^3 with $I_{xy} = 0$ is then calculated using (44). The solution of the bending stress for the profile contour ($0 \leq t \leq 2\pi$) in the rotated coordinate system is obtained using (48) as follows:

$$\sigma_z = \frac{M_b}{82113}\xi(\phi, t), \tag{50}$$

with

$$\xi(\phi, t) = r\sin(t - \phi) + \tfrac{1}{8}e_0(40\sin(7t - \phi) + 11\sin(13t - \phi) - 28\sin(5t + \phi) + 13\sin(11t + \phi)). \tag{51}$$

By substituting Equation (52) into Equation (51), the following relationship can be obtained for the distribution of the bending stress on the lateral surface of the profiled shaft for an arbitrary rotation angle ϕ:

$$\sigma_b(t) = \tfrac{17.44M_b}{82113} \cdot [\sin(t - \phi) + 0.089\sin(7t - \phi) + 0.0245\sin(13t - \phi) - 0.0623\sin(5t + \phi) + 0.02892\sin(11t + \phi)]. \tag{52}$$

In addition, numerical investigations were carried out using FEA to compare with Equation (52). The MSC-Marc programme system was used. Figure 8 shows the mesh structure and the corresponding boundary conditions. The profiled shaft is fixed on the left side. The bending moment is transferred to the shaft's right side via a reference node using REB2. The FE mesh contains 185,280 hexahedral elements with full integration (type 7 according to the Marc Element Library [17]) and 202,258 nodes. The FE meshes were generated with the help of software written in Python language at the Chair of Machine Elements at the West Saxon University of Applied Sciences in Zwickau. The FE meshes were then transferred to the MSC-Marc program system and integrated into the pre-processing.

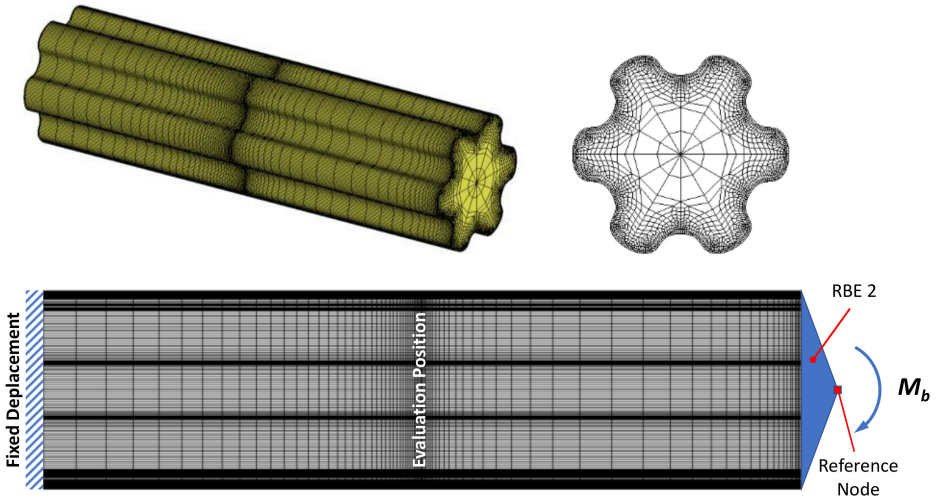

Figure 8. FE mesh and boundary conditions for the M-T04 profile.

The stress distribution is determined for two angles of rotation ($\phi = 0$ and $\phi = \pi/2$) using Equation (52) and compared with the results of the finite-element (FE) analyses in Figure 9, where $M_b = 500$Nm. As shown, the results agree well.

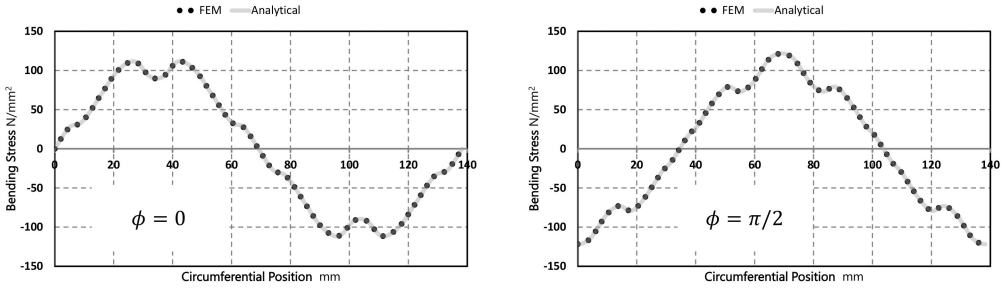

Figure 9. Distribution of the bending stresses on the M-T04 profile for two rotation angles: FEM results and analytical solution based on Equation (52).

Figure 10 presents the bending stresses on the profile contour for different rotation angles, which were determined using Equation (52). As expected, the maximum stress occurred at $\phi = \pi/2$ (or $\phi = \pi/6$) on the profile head.

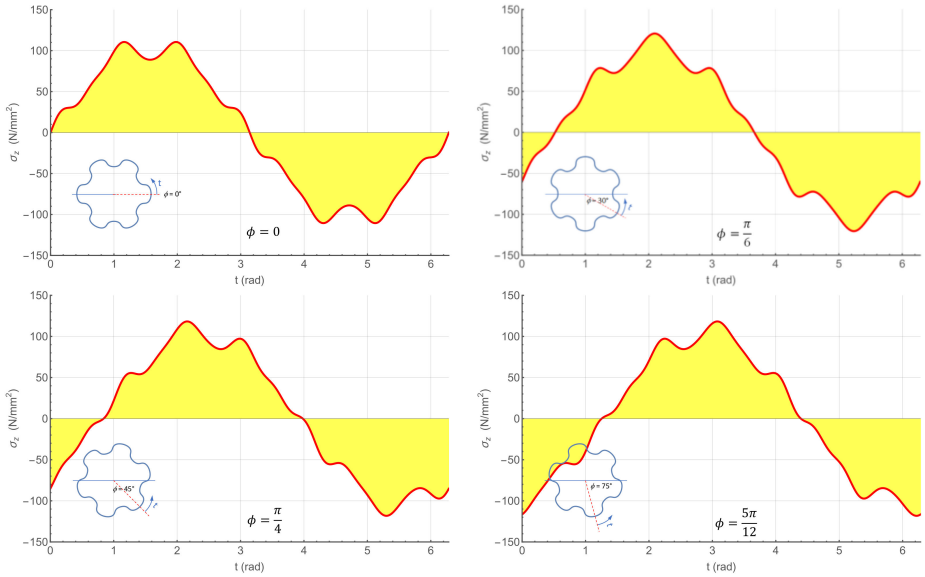

Figure 10. Distribution of the bending stresses on the M-T04 profile for several rotation angles according to Equation (52).

5.4. Modified M-04 Profile Based on [2]

In another transfer project with industry [2], the M-04 profile was modified for practical application as a shaft–hub connection in a transmission system. The geometric properties of the modified contour were $n = 6, r = 18.832$ mm, and $e_0 = 0.1416$ mm (Figure 11).

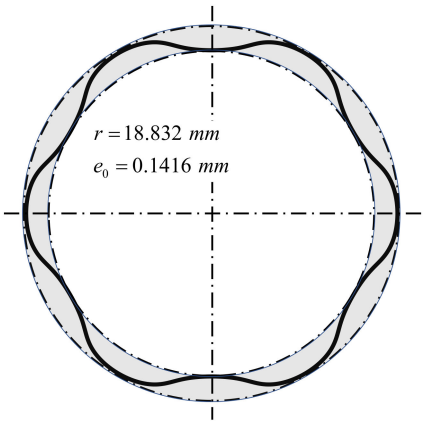

Figure 11. Modified M-T04 profile investigated in [2].

According to Equation (23), the contour of this profile is expressed as follows:

$$\omega(\zeta) = -\frac{0.231}{\zeta^{11}} + \frac{0.497}{\zeta^5} + 18.832\zeta + 0.71\zeta^7 + 0.195\zeta^{13}. \tag{53}$$

From (44), the bending moment of inertia is determined as $I_x = I_y = 100920$ mm^3 and $I_{xy} = 0$ mm^3.

The solution for the bending stress for the profile contour ($0 \leq t \leq 2\pi$) in a rotated coordinate system is obtained using (48) as follows:

$$\sigma_z = \frac{M_b}{100920}\xi(\phi, t). \tag{54}$$

By substituting ξ from Equation (51) into Equation (54), the following relationship can be obtained for the distribution of the bending stress on the lateral surface of the profiled shaft for an arbitrary rotation angle ϕ:

$$\begin{aligned}\sigma_b(t) = \tfrac{18.832M_b}{100820} \cdot [&\sin(t-\phi) + 0.0376\sin(7t-\phi) + 0.0103\sin(13t-\phi) - \\ &0.0263\sin(5t+\phi) + 0.0122\sin(11t+\phi)].\end{aligned} \tag{55}$$

The distribution of the bending stress was determined for two angles of rotation ($\phi = 0$ and $\phi = \pi/2$) using Equation (55) and compared with the results of the FE analyses, as shown in Figure 12, where $M_b = 500$ Nm. Good agreement between the results was observed.

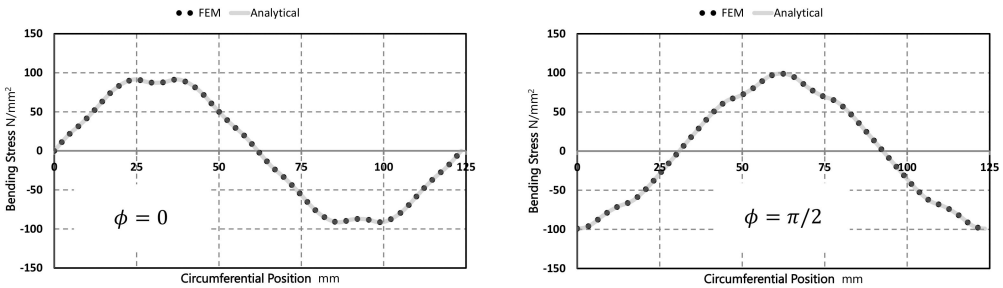

Figure 12. Distribution of the bending stresses on the M-T04 profile for two rotation angles: FEM results and analytical solution based on Equation (55).

5.5. Experimental Investigations

In addition to analytical and numerical solutions, experimental measurements were performed using strain gauges (Figure 13 left). A comparison of the experimental results with the solution obtained using Equation (36b) is presented in Figure 13 right; as shown, good agreement was observed.

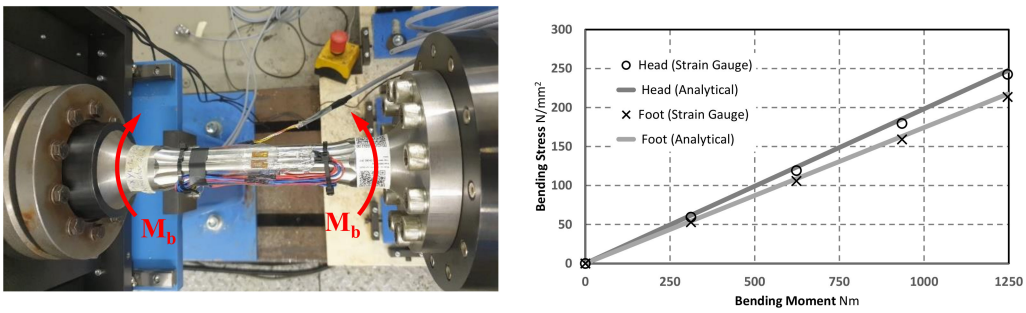

Figure 13. Testbench for the bending load, with a strain-gauge application (**left**); comparison of the analytical solution of Equation (55) with the experimental data (**right**) [2].

5.6. Deflection

The deflection can be easily determined from Equation (36a) as a function of the axial coordinate:

The shaft deflection was calculated for both M-04 [1] and the modified profile [2] for a length of $l = 140$ mm, with $M_t = 500$ Nm and an elastic modulus of $E = 210000$ N/mm^2 for steel. Figure 14 presents the deflection for both shaft profiles and a comparison with the numerical (FE analysis) results; as shown, good agreement was observed.

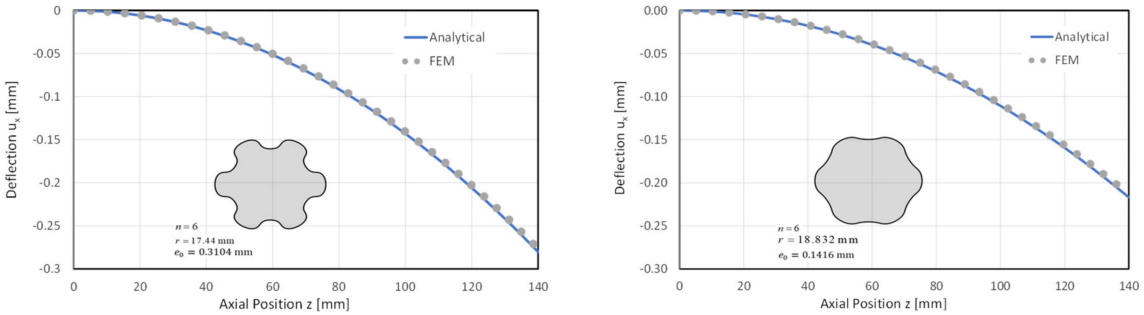

Figure 14. Shaft deflection of the M-04 [1] (**left**) and the modified profile [2] (**right**): comparison between the FE analysis results and the results based on Equation (36c).

6. Conclusions

The geometric characteristics of the higher trochoids were systematically discussed in the first part of this paper. The advantages of such profiles, known as the M-T04 profile family, were represented for use as shaft–hub connections.

Because of a practical viewpoint, the geometrical features, such as head circle, root circle, tooth height, etc., were described analogously to the standardised tooth profiles for shaft-hub connections. In contrast to the standard tooth profiles, the higher trochoids have mathematically continuous contours.

The next part of the paper outlined a general theory of bending-loaded profile shafts. A general solution of the rotating bending stress and deformations for pure bending (without shear force) was presented. By properly formulating the geometric-mechanical relations of the trochoidal curves with the help of complex functions, closed solutions for the bending stresses and the elastic deformations in such profiles were derived. The obtained equations allow a quick design of the profiled shaft with the help of a simple pocket calculator without expensive FE analyses. The solution was directly applied to two M-04 profiles. The analytical results agreed very well with numerical and experimental findings.

Funding: This research was funded by DFG (Deutsche Forschungsgemeinschaft) grant number [DFG ZI 1161/3].

Institutional Review Board Statement: Not applicable.

Informed Consent Statement: Not applicable.

Data Availability Statement: The study will be published soon (still in 2022) on https://fis.fh-zwickau.de/ (accessed on 28 June 2022).

Acknowledgments: The author thanks the German Research Foundation (Deutsche Forschungsgemeinschaft DFG) for funding the research projects DFG ZI 1161/1-1 and DFG ZI 1161/3, which made this study possible.

Conflicts of Interest: The authors declare no conflict of interest.

Nomenclature

Formula symbols

$\boldsymbol{A}$	mm^2	Area of profile cross-section
$\boldsymbol{e}$	mm	Profile eccentricity
$\boldsymbol{e_{grenz}}$	mm	Profile overlap eccentricity limit
$\boldsymbol{E}$	MPa	Young's modulus
$\boldsymbol{n}$	-	Profile periodicity (number of sides)
$\boldsymbol{I_p}$	mm^4	Polar moment of inertia
$\boldsymbol{I_x, I_y, I_{xy}}$	mm^4	Surface moments of inertia in a Cartesian coordinate system
$\boldsymbol{I_\xi, I_\eta, I_{\xi\eta}}$	mm^4	Surface moments of inertia in a rotated coordinate system
$\boldsymbol{l}$	mm	Length of profiled shaft
$\boldsymbol{M_b}$	Nm	Bending moment
$\boldsymbol{r}$	mm	Nominal or mean radius
$\boldsymbol{t}$	-	Profile parameter angle
$\boldsymbol{u_x, u_y, u_z}$	mm	Displacement components
$\boldsymbol{x, y, z}$	mm	Cartesian coordinates

Greek formula symbols:

$\varepsilon = e_0/r$	-	Relative eccentricity
ϕ	-	Rotation angle of a coordinate system
$\lambda = e^{i\theta}$	-	Physical plane unit circle
θ	-	Polar angle
σ_b, σ_z	MPa	Bending stress (z-component of stress vector)
$\omega(\zeta)$	-	Completed mapping function
$\omega_0(\zeta)$	-	Contour edge mapping function
ζ	-	Complex variable in model plane
ξ, η	-	Coordinates in rotated system

References

1. *Research Report: Entwicklung Kontinuierlicher Unrunder Innen- und Aussenkonturen für Formschlüssige Welle-Nabe-Verbindungen und Ermittlung Analytischer Lösungsansätze*; Abschlussbericht zum DFG-Vorhaben DFG ZI 1161/1; Westsächsische Hochschule Zwickau: Zwickau, Germany, 2016.
2. *Research report: Einsetzen der Trochoidischen Konturen für Formschlüssige Welle-Nabe-Verbindungen in Antriebstechnik*; DFG-Vorhaben DFG ZI 1161/3; Laufend, Westsächsische Hochschule Zwickau: Zwickau, Germany, 2022.
3. *DIN 32711:2009-03*; Welle-Nabe-Verbindung—Polygonprofil P3G—Teil 1: Allgemeines und Geometrie. DIN-Deutsches Institut für Normung e.V.: Berlin, Germany, 2009.
4. *DIN 5480-2:2015-03*; Passverzahnungen mit Evolventenflanken und Bezugsdurchmesser—Teil 2: Nennmaße und Prüfmaße. DIN-Deutsches Institut für Normung e.V.: Berlin, Germany, 2015.
5. *DIN 3689-1:2021-11*; Welle-Nabe-Verbindung—Hypotrochoidische H-Profile—Teil 1: Geometrie und Maße. DIN-Deutsches Institut für Normung e.V.: Berlin, Germany, 2021.
6. Muskelishvili, N.I. *Some Basic Problems of the Mathematical Theory of Elasticity*; Springer: Dordrecht, The Netherlands, 1977.
7. Wunderlich, W. *Ebene Kinematik*; Bibliographisches Institut Mannheim: Stuttgard, Germany, 1968.
8. Zwikker, C. *The Advanced Geometry of Plane Curves and Their Applications*; Dover Books on Advanced Mathematics; Dover: Mineola, NY, USA, 1963.

9. Ziaei, M.; Selzer, M. Analytische Ansätze zur Ermittlung der Torsionsbeanspruchung und der Kerbwirkungszahl in Wellen mit kontinuierlichen unrunden Konturen. In Proceedings of the VDI-Tagung Welle-Nabe-Verbindungen, Stuttgart, Germany, 26–27 November 2018.
10. Sokolnikoff, I.S. *Mathematical Theory of Elasticity*; Robert, E., Ed.; Krieger Publishing Company: Malaba, FL, USA, 1983.
11. Ziaei, M. Torsionsspannungen in Prismatischen, Unrunden Profilwellen mit Trochoidischen Konturen, Forschung im Ingenieurwesen, Ausgabe 4/2021, Germany, Professional Journal. Available online: https://www.researchgate.net/publication/355421692_Torsionsspannungen_in_prismatischen_unrunden_Profilwellen_mit_trochoidischen_KonturenTorsional_stresses_and_deformations_in_prismatic_non-circular_profiled_shafts_with_trochoidal_contours (accessed on 28 June 2022).
12. Ziaei, M. *Analytische Untersuchung Unrunder Profilfamilien und Numerische Optimierung Genormter Polygonprofile für Welle-Nabe-Verbindungen „Habilitationsschrift"*; Technische Universität Chemnitz: Chemnitz, Germany, 2002.
13. Selzer, M.; Ziaei, M. Zykloiden höherer Stufe—Alternative für formschlüssige Welle-Nabe-Verbindungen Teil 1. „antriebstechnik" Heft 10/2016 S.100, Vereinigte Fachverlage. In Proceedings of the VDI Meeting on Shaft Hub Connection, Oktober 2016.
14. Selzer, M.; Ziaei, M. Zykloiden höherer Stufe—Alternative für formschlüssige Welle-Nabe-Verbindungen Teil 2. „antriebstechnik" Heft 03/2017 S.66, Vereinigte Fachverlage. In Proceedings of the VDI Meeting on Shaft Hub Connection, March 2017.
15. Brown, J.W.; Churchill, R.V. *Complex Variables*, 9th ed.; McGraw-Hill: New York, NY, USA, 2013.
16. Hibbeler, R.C. *Engineering Mechanics, Statics*, 14th ed.; Pearson Prentice Hall Pearson Education, Inc.: Hoboken, NJ, USA, 2016.
17. *Marc 2020 Manual*; Element Library; MSC Software Corporation: Newport Beach, CA, USA, 2020; Volume B.